AGU PUBLICATIONS

JGR

Journal of Geophysical Research: Space Physics

RESEARCH ARTICLE

10.1002/2014JA019773

Key Points:

- An isolated substorm was preceded by a PBI, flow channel, and waves
- Precursor weak waves are found to connect to onset waves
- We suggest a coupling process of preonset waves and flows for onset instability

Correspondence to:
Y. Nishimura,
toshi@atmos.ucla.edu

Citation:
Nishimura, Y., et al. (2014), Coordinated ionospheric observations indicating coupling between preonset flow bursts and waves that lead to substorm onset, *J. Geophys. Res. Space Physics*, *119*, 3333–3344, doi:10.1002/2014JA019773.

Received 8 JAN 2014
Accepted 14 APR 2014
Accepted article online 16 APR 2014
Published online 1 MAY 2014

Coordinated ionospheric observations indicating coupling between preonset flow bursts and waves that lead to substorm onset

Y. Nishimura[1], L. R. Lyons[1], M. J. Nicolls[2], D. L. Hampton[3], R. G. Michell[4], M. Samara[4], W. A. Bristow[3], E. F. Donovan[5], E. Spanswick[5], V. Angelopoulos[6], and S. B. Mende[7]

[1]Department of Atmospheric and Oceanic Sciences, University of California, Los Angeles, California, USA, [2]Center for Geospace Studies, SRI International, Menlo Park, California, USA, [3]Geophysical Institute, University of Alaska Fairbanks, Fairbanks, Alaska, USA, [4]Department of Space Science and Engineering, Southwest Research Institute, San Antonio, Texas, USA, [5]Department of Physics and Astronomy, University of Calgary, Calgary, Alberta, Canada, [6]Department of Earth and Space Sciences, University of California, Los Angeles, California, USA, [7]Space Science Laboratory, University of California, Berkeley, California, USA

Abstract A critical, long-standing problem in substorm research is identification of the sequence of events leading to substorm expansion phase onset. Recent Time History of Events and Macroscale Interactions during Substorms (THEMIS) all-sky imager (ASI) array observations have shown a repeatable preonset sequence, which is initiated by a poleward boundary intensification (PBI) and is followed by auroral streamers moving equatorward (earthward flow in the plasma sheet) and then by substorm onset. On the other hand, substorm onset is also preceded by azimuthally propagating waves, indicating a possible importance of wave instability for triggering substorm onset. However, it has been difficult to identify the link between fast flows and waves. We have found an isolated substorm event that was well instrumented with the Poker Flat incoherent scatter radar (PFISR), THEMIS white-light ASI, and multispectral ASI, where the auroral onset occurred within the PFISR and ASI fields of view. This substorm onset was preceded by a PBI, and ionospheric flows propagated equatorward from the polar cap, crossed the PBI, and reached the growth phase arc. This sequence provides evidence that flows from open magnetic field lines propagate across the open-closed boundary and reach the near-Earth plasma sheet prior to the onset. Quasi-stable oscillations in auroral luminosity and ionospheric density are found along the growth phase arc. These preonset auroral waves amplified abruptly at the onset time, soon after the equatorward flows reached the onset region. This sequence suggests a coupling process where preexisting stable waves in the near-Earth plasma sheet interact with flows from farther downtail and then evolve to onset instability.

1. Introduction

Substorms are a dramatic disturbance of the global magnetosphere-ionosphere system that release large amounts of solar wind energy accumulated in the magnetotail [e.g., *Rostoker et al.*, 1980] and are associated with auroral activations [*Akasofu*, 1964]. Substorm expansion phase onset is characterized in the aurora by initial brightening that occurs along a preexisting, growth phase arc that emerges near the equatorward boundary of the auroral oval [*Akasofu*, 1964; *Samson et al.*, 1992; *Deehr and Lummerzheim*, 2001]. The growth phase arc is latitudinally narrow and oriented approximately in the east-west direction. The arc stays dim for a few to tens of minutes near the end of the growth phase [*Nishimura et al.*, 2011a] and then shows the first auroral signature of substorm onset, which is initial brightening that often appears as beads along this arc [e.g., *Donovan et al.*, 2006; *Liang et al.*, 2008; *Henderson*, 2009; *Rae et al.*, 2010]. The beads can be seen simultaneously in both hemispheres with similar wavelengths and periodicities [*Motoba et al.*, 2012], indicating that the beads are generated near the equatorial plasma sheet rather than in the auroral acceleration region or in the ionosphere. Otherwise, different ionospheric conditions would create different characteristics of waves in the different hemispheres. The auroral beads propagate azimuthally and evolve into wavy structures, indicating that the beads are an auroral manifestation of onset waves.

Additionally, highly fluctuating magnetic fields in the near-Earth plasma sheet have been suggested to be linked to a magnetospheric substorm onset instability [*Takahashi et al.*, 1987; *Lui*, 1995; *Ohtani et al.*, 1998; *Shiokawa et al.*, 2005]. The longer period component of those fluctuations (several tens of seconds) seems to correspond to periods seen in the aurora as the beads pass overhead. While the oscillations in the tail have not been connected to optical onset waves/beads, demonstration of such a connection would suggest that both may be signatures of what can be referred to as the "substorm onset instability."

Historically, the wave features in the near-Earth plasma sheet have been considered as indications of near-Earth initiation of the substorm sequence, which then evolves tailward (so-called inside-out scenario). However, a number of studies showed that enhanced earthward plasma flows are present prior to substorm onset [*Sergeev et al*., 1995; *Shiokawa et al*., 1998; *Baker et al*., 2002; *Angelopoulos et al*., 2008; *Machida et al*., 2009; *Miyashita et al*., 2009; *Kepko et al*., 2009], which supports the outside-in scenario. Moreover, auroral observations from the Time History of Events and Macroscale Interactions during Substorms (THEMIS) all-sky imager (ASI) network have shown that substorm expansion phase onset is preceded by poleward boundary intensifications (PBIs) followed by north-south oriented auroral streamers propagating toward the substorm onset location and then leading to substorm onset [*Nishimura et al*., 2010a]. Note that auroral streamers have been known to be the ionospheric manifestation of plasma sheet flow bursts [*Henderson et al*., 1998; *Sergeev et al*., 2000; *Nakamura et al*., 2001; *Kauristie et al*., 2003], where upward field-aligned currents form on the duskside edge of flow bursts and can be measured as discrete aurora [*Birn et al*., 2004; *Yang et al*., 2012].

These studies suggest that substorm onset may really be a hybrid of the old "inside-out" and "outside-in" scenarios, where the incoming flow bursts (outside-in component) change conditions within the inner plasma sheet and lead to the substorm onset instability and following expansion phase activity (inside-out component). Of further potential interest to such an onset scenario, recent observations have found waves prior to substorm onset in the near-Earth plasma sheet [*Saito et al*., 2008; *Panov et al*., 2012] and in optical observations in the vicinity of onset locations [*Uritsky et al*., 2009]. These waves do not immediately grow upon their appearance but are relatively stable until the onset. The above phenomena (relatively stable preonset auroral waves, preonset flow channels, auroral beading, and the magnetospheric waves), if they can be shown to couple together, provide critical clues for understanding what leads to substorm onset instability in the near-Earth plasma sheet. However, due to the limited number of observation points, it has been difficult to evaluate if they are all linked or occur independently.

The purpose of the present study is to determine if these connections exist, and if so, what the fundamental features of the connections are. We use ground-based ASIs and the Poker Flat incoherent scatter radar (PFISR). These provide 2-D spatial coverage and allow tracing of optical, density, and flow features, in contrast to what can be obtained from satellite measurements. During the recent PFISR radar campaigns, called PFISR Ion Neutral Observations in the Thermosphere (PINOT), PFISR was operated for much longer time intervals than usual (12 and 16 continuous nights) in special operation modes, together with supporting instruments including high-resolution colored ASIs. A remarkable, isolated substorm occurred on 7 November 2012 during the campaigns, the onset initiating within the PFISR field of view (FOV) during a period of dense spatial coverage by 41 radar beams. The auroral oval was quite thin near the onset time, so that the entire latitudinal width of the oval was located within the single radar FOV, and the entire sequence of events around the onset meridian was covered by the radar. We find that preonset faint waves grew rapidly and evolved to onset beads soon after equatorward flows reached the onset region. We suggest that this auroral wave growth is a manifestation of the substorm onset instability and that the interaction between the preonset waves in the near-Earth plasma sheet and the fast earthward flows leads to this instability.

2. Data Set

2.1. PFISR Radar

The PFISR radar is part of the Advanced Modular Incoherent Scatter Radar project in Poker Flat [*Nicolls and Heinselman*, 2007]. The radar provides the ionospheric density and line-of-sight (LOS) velocity on a designated pattern of beams. The beam pattern during this PINOT campaign consists of 41 beams, which are split into five meridians (Figure 1a). The time resolution with a favorable signal-to-noise ratio depends on backscatter echo intensities (i.e., ionospheric density), and in this event we use 20 s resolution for obtaining reliable physical quantities. This resolution is sufficiently high to detect $> \sim 1$ min time scale changes associated with PBIs, streamers, and preonset waves.

Some plots used in this study combine beams along each meridian to remove the latitude and altitude ambiguity. When showing data in a latitude-time format, we calculated the peak density and median flow speed in the *F* region of the ionosphere (between 130 and 400 km altitude) at each latitude and time. We

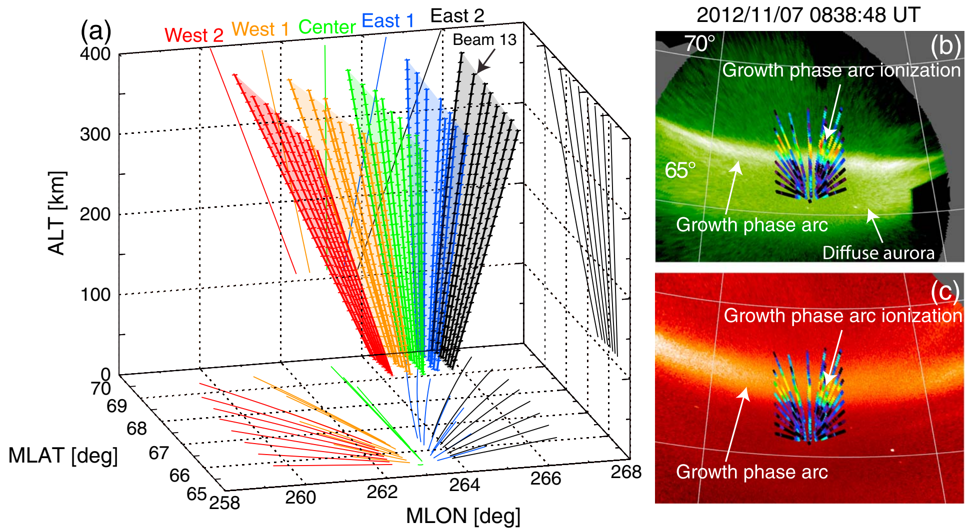

Figure 1. (a) PFISR 3-D beam pattern during this event. Beams are classified into five meridians for the purpose of this study. (b and c) PFISR density data plotted on top of 557.7 and 630.0 nm images.

excluded flow data when densities are less than $7 \cdot 10^{10}$ (/m^6), a threshold below which the data become noisy at these short integration times. For density data in an altitude-time format, the peak density within a specified latitude range was calculated. When mapping radar data onto 2-D imager snapshots, the radar data were mapped along the magnetic field lines to a reference altitude. The altitude adjustment corrected geomagnetic (AACGM) coordinates are used throughout this study so that we can compare values at different altitudes along each magnetic field line.

2.2. All-Sky Imagers

Our optical observations were performed mainly using a multispectral electron-multiplying CCD camera in Poker Flat [*Samara and Michell*, 2010]. The high-resolution observations (~500 m in space near zenith and 3 Hz in time) at 557.7 (green) and 630.0 (red) nm allow detecting auroral emissions associated with high- and low-energy precipitation. This high spatial and temporal resolution and the camera's low noise levels (approximately a few Rayleighs) allow detecting auroral forms of interest, including preonset waves, which typically have ~100 km size, ~1–2 min periodicity, and intensities of a few tens of Rayleighs.

Projection altitudes of the imager data were determined by referring to the PFISR density observations. As shown in section 3, the bottom edge of the growth phase arc ionization (representing high-energy precipitation seen in 557.7 nm) is located at ~150 km altitude, and the peak ionization altitude (from lower energy precipitation seen in 630.0 nm) is at ~230 km. We thus used 150 and 230 km for plotting the 557.7 and 630.0 nm data, respectively, in AACGM as shown by the example in Figures 1b and 1c. Also shown is the PFISR density data mapped to the 150 km altitude of the 557.7 nm emissions. The PFISR mapping altitude does not significantly affect comparison with the 630.0 nm emissions, since the magnetic field lines are oriented almost vertically. The low-altitude edge of the enhanced density in the radar data (which is the low-latitude edge of the mapped data because of the poleward looking beams) coincides well with the growth phase arc seen in the 557.7 nm wavelength, and the peak density location correspond to the arc in the 630.0 nm wavelength. This agreement validates our mapping approach for comparing the radar and optical data.

In our study, PBIs are defined as auroral intensifications along the poleward boundary of the auroral oval in the 630.0 nm imager data. Preonset waves are identified as quasi-periodic luminosity modulations along the growth phase arc of ~1 min periods [*Uritsky et al.*, 2009]. Onset is identified from the initiation of waves seen as beads along the growth phase arc that rapidly intensify and expand poleward [*Donovan et al.*, 2006; *Liang et al.*, 2008]. This onset definition is also consistent with that by *Akasofu* [1964], where onset is defined as initial brightening along a growth phase arc near the equatorward boundary of the auroral oval and is followed by poleward expansion. Azimuthal separations of preonset and onset waves are typically between several tens of kilometers and a few hundreds of kilometers, which can be well resolved by the imagers.

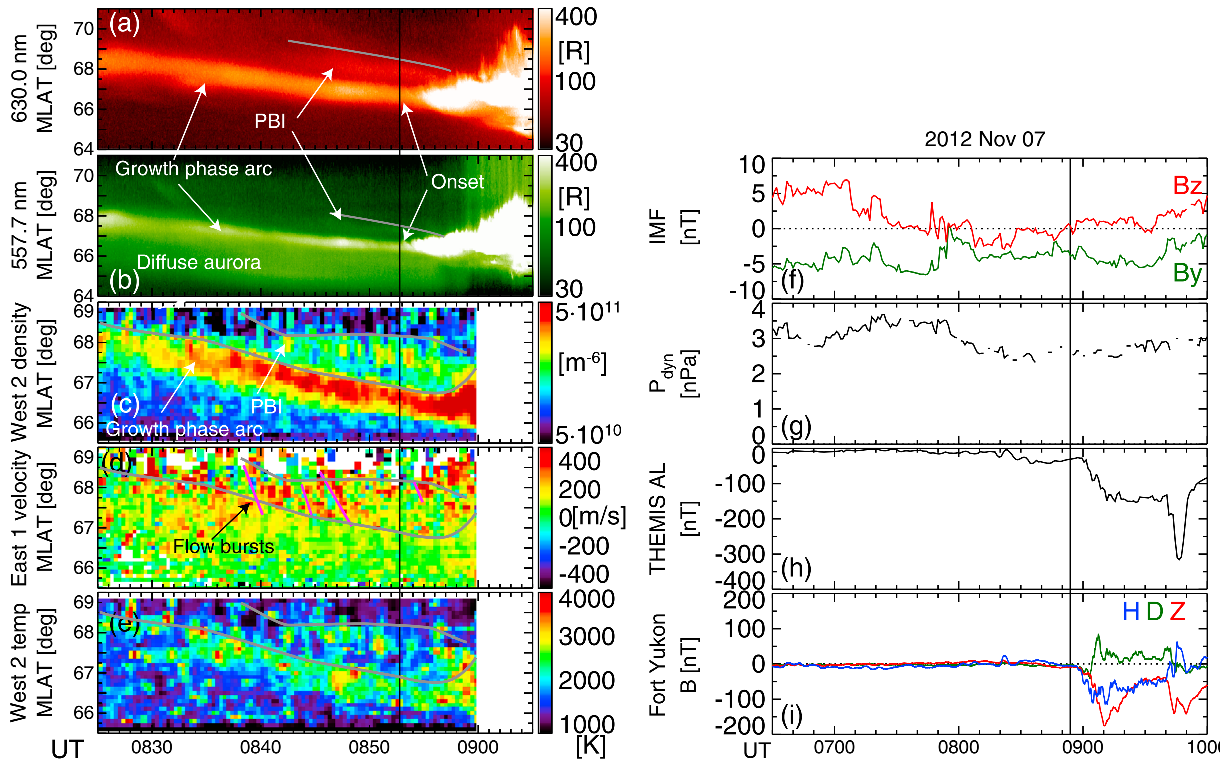

Figure 2. The (a) 630.0 and (b) 557.7 nm imager keogram near the onset meridian (averaged over 1.5° MLON). A constant intensity of 400 R is subtracted from original data for showing dim features more clearly. The white data points indicate intensity above the color scale. (c) PFISR density from the West 2 meridian, (d) LOS velocity from the East 1 meridian (positive toward the radar), and (e) electron temperature from the West 2 meridian. The gray lines visually trace flow bursts and poleward boundaries of the growth phase arc and PBI arc. The lack of radar data after 0900 UT is due to the operation mode change. The magenta lines identify the flow bursts. (f) OMNI IMF, (g) solar wind dynamic pressure, (h) THEMIS *AL*, and (i) ground magnetometer data at Fort Yukon. The color scales in Figures 2a–2c are logarithmic.

To identify dim auroral features clearly in 2-D snapshots and north-south keograms, we subtracted a constant intensity (400 R) from all imager pixels and show them in a logarithmic scale. East-west keograms were created by slicing data along the growth phase arc, and 3 min averages were subtracted.

For a reference to white-light signatures, we also use one of the THEMIS ASIs at Fort Yukon, which is located at ~150 km northeast of Poker Flat. The spatial resolution near the zenith is ~1 km, and the time resolution is 3 s [*Mende et al.*, 2008].

3. Results

3.1. Event Overview

Figure 2 shows the sequence of this substorm. The time series of 557.7 (Figure 2a) and 630.0 (Figure 2b) nm are displayed as keograms near the onset meridian averaged over 1.5° magnetic longitude (MLON). Prior to the onset, a quiet auroral oval can be seen that slowly drifted equatorward, a typical signature of the substorm growth phase. A faint intensification (seen more clearly in 630.0 nm) occurred just poleward of the growth phase arc ~10 min prior to the onset. This can be recognized as a PBI since no significant intensification is found poleward of this. While the oval was much narrower than usual, several examples of such thin oval events have been reported previously [*Lyons et al.*, 2010; *Nishimura et al.*, 2011b]. Due to the thin oval, the latitude separation between the PBI and growth phase arc was too small to examine if steamers were present. Then the growth phase arc suddenly intensified (marking the substorm onset at 0852:50 UT) and expanded poleward. The latitudinal profile of the electron density (Figure 2c) obtained from the eight beams nearest to the onset meridian (West 2 in Figure 1a) shows a striking resemblance to the optical measurements: two high-density structures can be seen that correspond to the growth phase arc and to the PBI. The elevated electron temperatures (Figure 2e) in both high-density regions indicate that these are due to precipitating particles rather than remnants of plasma flowing from elsewhere. The density started to increase at the onset time,

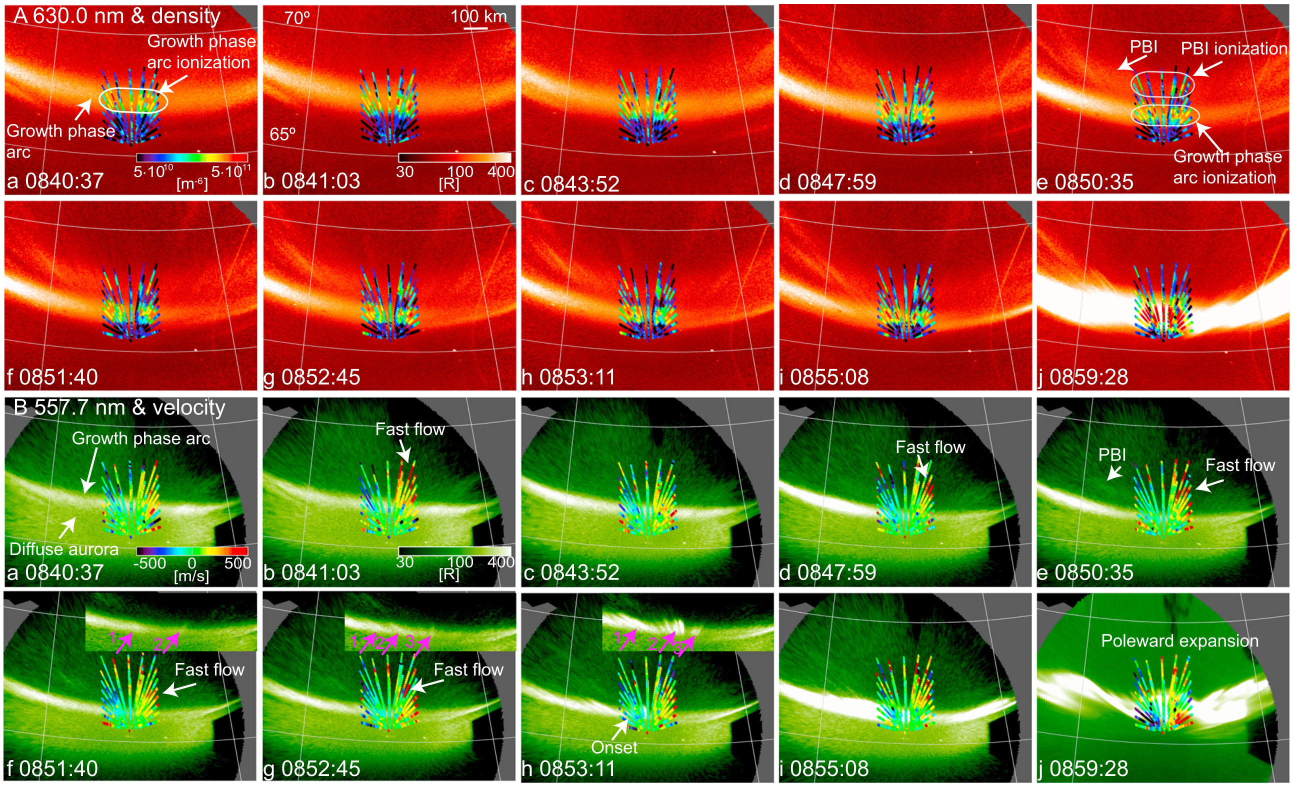

Figure 3. Snapshots of (A) 630.0 nm and density and (B) 557.7 nm and LOS velocity data. The inserts in Figures 3Bf–3Bh show blowups of the growth phase arc around the onset location.

and the increase then expanded poleward. The sharp density gradient at the poleward edge of the poleward enhanced density (indicated by the poleward gray line) supports the location of the poleward boundary of the auroral oval indicated by 630.0 nm observations (grey line in Figure 1a). Thus, the whole latitudinal extent of the auroral oval was covered by the PFISR FOV. The two arcs appear to be separated latitudinally during the growth phase, and it is difficult to find if streamers were present between the two arcs due to the narrow auroral oval. On the other hand, the LOS velocity from the East 1 beams (Figure 2d) clearly shows multiple preonset flow bursts (identified by tilted magenta lines) that propagated toward lower latitudes and reached the poleward portion of the growth phase arc ionization. Flow signatures are discussed more in detail in section 3.2. THEMIS *AL* and the magnetometer data at Fort Yukon (Figures 2h and 2i) show an auroral electrojet enhancement soon after the auroral onset. The time lag corresponds to a finite time to grow the electrojet intensity to an observable level, and this has also been seen in other events [e.g., *Lyons et al*., 2013]. There was no substantial electrojet activity until the onset time other than a small THEMIS *AL* decrease after the interplanetary magnetic field (IMF) B_z turned southward (growth phase). The quiet magnetic field and aurora prior to the onset indicate that this is an isolated substorm.

Figure 3 shows selected 2-D snapshots of imager and radar data. The 630.0 nm images in Figure 3A shows the east-west oriented growth phase arc, which stayed quiet and slowly drifted equatorward, and then a separate arc (PBI arc) emerged just poleward of it. Those arcs are well collocated with the two bands of enhanced density in the PFISR data, which are overlaid on the 630.0 nm images. The PFISR LOS flow data are overlaid on the 577.7 nm images in Figure 3B and show transient and localized fast flows poleward of the growth phase arc during this period. A flow burst suddenly emerged in Figure 3Bb and reached the poleward portion of the growth phase arc. The flow burst disappeared by the time of Figure 3Bc, and more flow bursts were detected in Figures 3Bd–3Bg. While the measurements are LOS, the presence of weak equatorward flows along the central meridian beams and the equatorward propagation seen in Figure 2d suggests that these fast flows had a significant equatorward component. The equatorward flows were limited mainly to the eastern half of the radar FOV and reached the growth phase arc just a few degrees to the east of the onset meridian, which was located in the western half of the radar FOV.

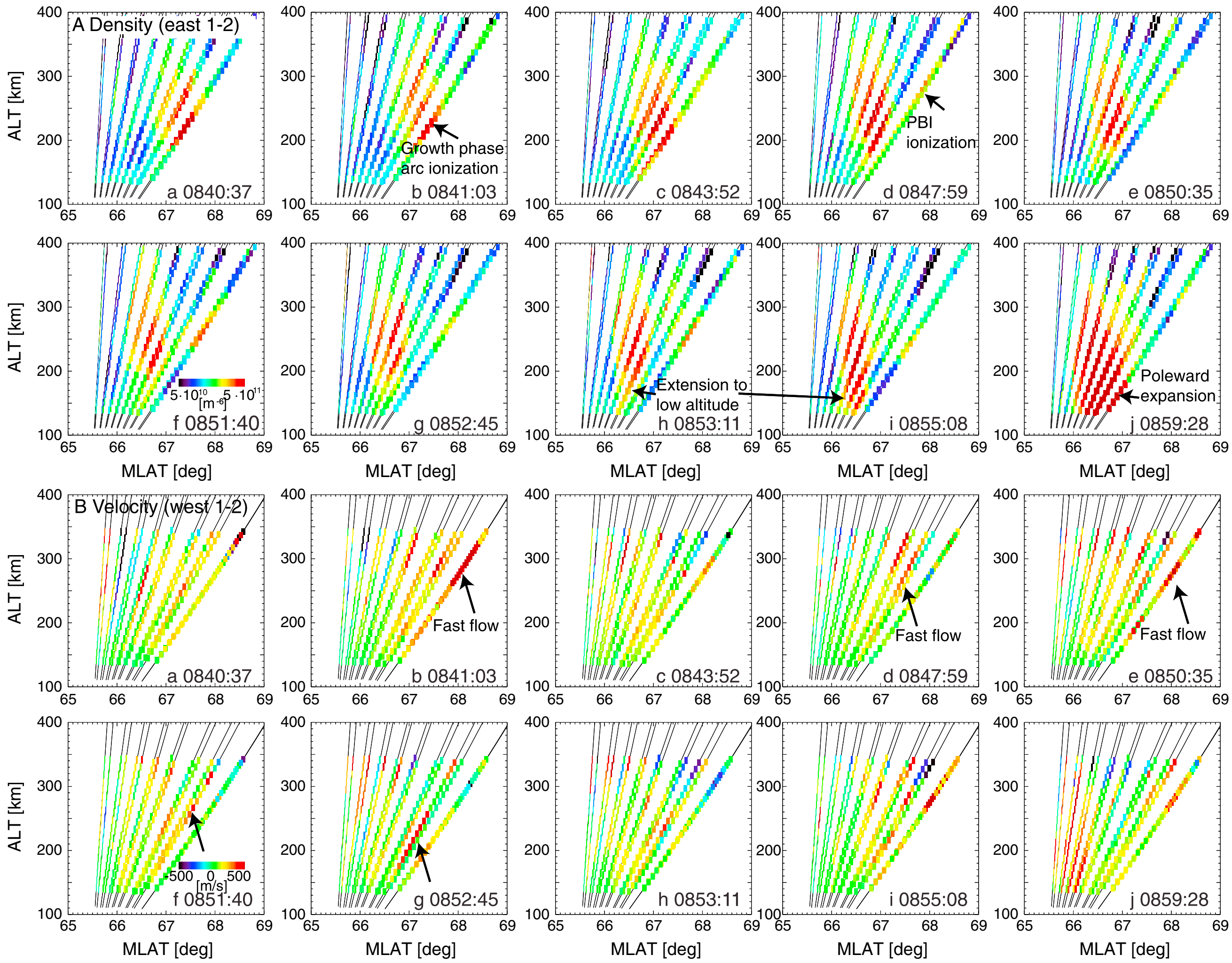

Figure 4. Altitude-latitude distribution of (A) density from West 1 and 2 beams and (B) LOS velocity from East 1 and 2 beams at the same times as in Figure 3.

While the luminosity of the growth phase arc is overall quite uniform with only small azimuthal variations, the blowup around the onset region given in the inset of Figure 3Bf shows faint and localized blobs of luminosity enhancements. Those blobs propagated westward and remained dim until the onset time (Figure 3Bg) and then rapidly intensified (Figure 3Bh). As discussed more in detail in section 3.3, the blob intensification marks the initiation of the onset beads, and interestingly, the beads are seen as an intensification of the preexisting faint blobs, meaning that the onset beads developed from the preexisting and relatively stable auroral blobs rather than as a separate feature.

While the optical observations integrate luminosity information along the LOS directions, PFISR data can provide altitude profiles of the density and velocity associated with the two arcs. Figure 4 shows density and velocity along the altitude and latitude planes by combining East 1 and 2 meridians (density) and West 1 and 2 meridians (velocity). The growth phase arc can be seen as a tall ionization structure that extends between ~150 and ~350 km with a peak density at ~200–250 km (Figure 4A), indicating that a broad energy range of precipitation leads to the growth phase arc. The growth phase arc slowly moved equatorward during the series of profiles in Figure 4A, and the PBI arc moved into the poleward portion of the radar FOV as identified in Figure 4Ad. While the low-altitude edge of the PBI ionization was still out of the FOV, the high-altitude edge was located at ~350 km, suggesting that low-energy precipitation contributed to the PBI.

The substorm onset is characterized as an abrupt extension of ionization to lower altitudes. Comparing Figures 4Ag and 4Ah shows that the density below 200 km was enhanced, while the density above 200 km changed only slightly. This altitude dependence is an indication that onset is associated with a sudden

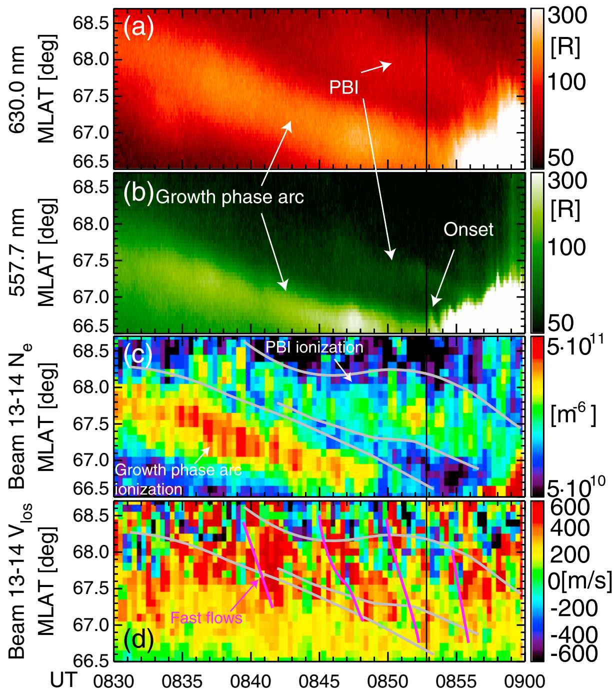

Figure 5. (a, b) Colored keograms (same as in Figure 2) and (c, d) the density and LOS velocity along beam 13. The gray lines visually trace ionization boundaries.

increase in high-energy precipitation, while the low-energy portion of precipitation did not significantly change. Then the density enhancement extended to a broad altitude range and also expanded poleward (Figures 4Ai and 4Aj).

In the eastern radar beams in Figure 4B, fast positive LOS flows can be seen between the growth phase arc and PBI arc and reach the poleward portion of the growth phase arc just before onset (Figure 4Bg). In addition, moderate LOS flows of ~200–300 m/s are found within and slightly equatorward of the growth phase arc. The flow equatorward of the growth phase arc was rapidly enhanced during the poleward expansion (Figure 4Bj).

3.2. Fast Flow Originating From the Polar Cap, Reaching the Growth Phase Arc, and Leading to Onset

In order to find the evolution of the fast flows more clearly, we show in Figure 5 radar data from beam 13, which is one of the East 2 beams as marked in Figure 1. While the density and velocity signatures are overall similar to those in the combined beams shown in Figure 2d, the flow bursts can be seen more clearly, particularly in the polar cap where the flow signatures are obscured in the previous figure due to the combination of multiple beams. Three of the

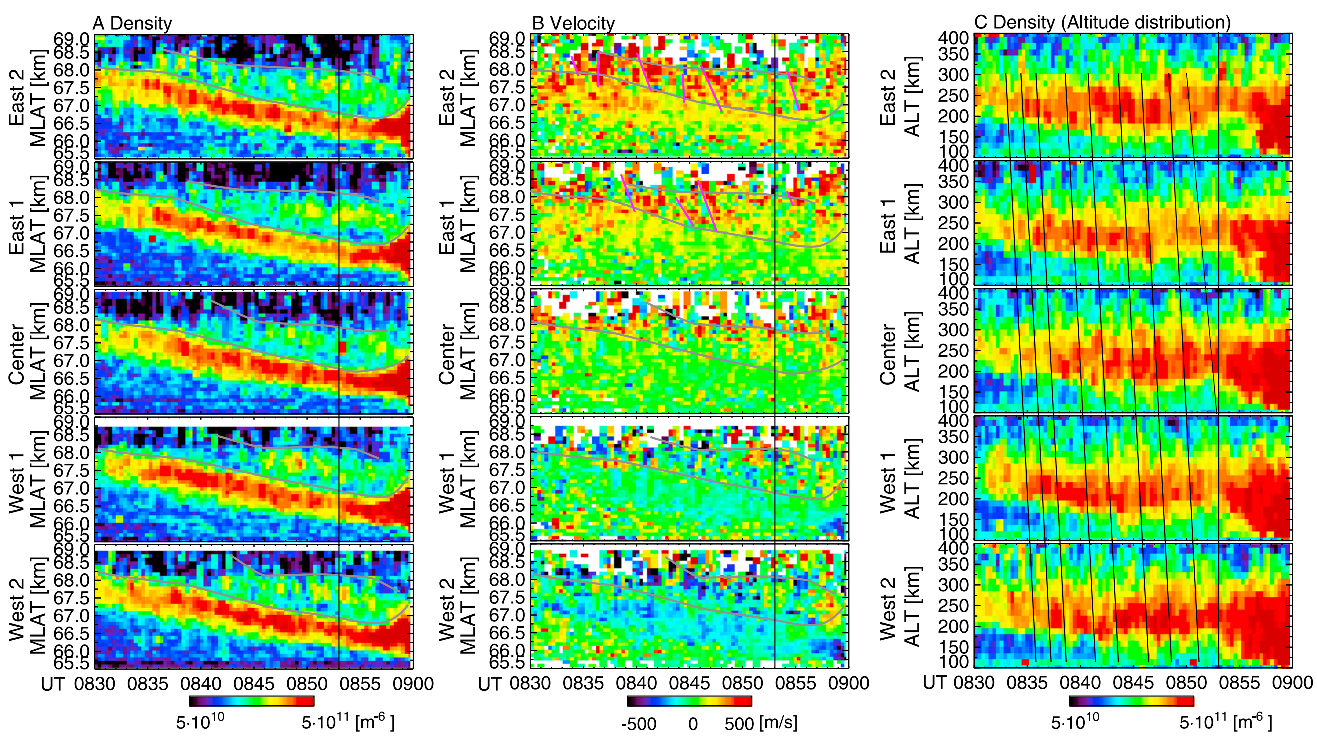

Figure 6. Latitude distribution of the (a) density and (b) LOS velocity from all five meridians. (c) Altitude distribution of density. The gray, magenta, and black lines mark the ionization boundaries, flow bursts, and westward propagating density, respectively.

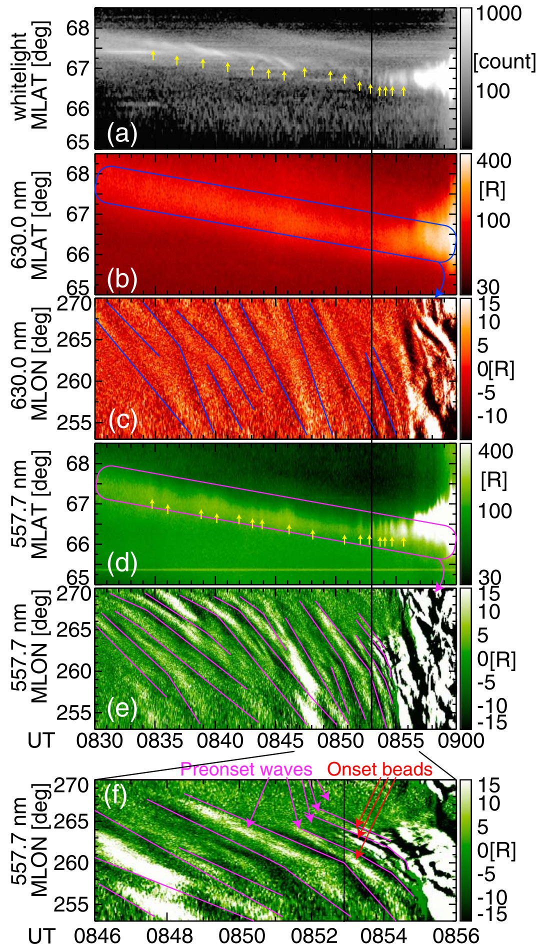

Figure 7. (a) White-light north-south keogram. The 630.0 nm data in the (b) north-south and (c) east-west keograms. The 557.7 nm data in the (d) north-south and (e) east-west keograms. (f) Blowup of Figure 7d around the onset time. The boxes in Figures 7b and 7d mark the latitude ranges used for Figures 7b and 7d, and 3 min sliding averages are subtracted. The keograms used 0.01° integrations over longitude. Lines in Figures 7c, 7e, and 7f visually trace optical waves.

flow bursts at 0844, 0845–0849, and 0851:30–0853 UT were seen first in the polar cap and then propagated equatorward across the PBI. The PBI arc and ionization remained separated from the growth phase arc and its ionization by ~0.2° magnetic latitude (MLAT), and weak and varying ionizations in this gap might be a signature of streamers, although we cannot be certain due to the limited data points in this gap. The flow bursts propagated farther equatorward of the PBI ionization and reached the poleward portion of the growth phase arc of the onset beads. The onset occurred just 2 min after the fourth flow burst reached the growth phase arc.

The existence of flows in the polar cap associated with the PBI is consistent with previous findings by radars [*Nishimura et al.*, 2010b; *Lyons et al.*, 2011; *Shi et al.*, 2012; *Pitkänen et al.*, 2013], and our observations show a continuous propagation sequence from the polar cap to the growth phase arc. These flows prior to the onset are likely the ionospheric signature of plasma sheet flows that have been seen prior to onset by satellites [e.g., *Angelopoulos et al.*, 2008]. The 2-D coverage of the radar and ASI observations allows us to identify the evolution of the preonset flow bursts from the polar cap to the substorm onset location soon before the onset.

Figure 6 shows a time series of density and velocity from all five meridians identified in Figure 1. As seen in Figure 3, Figure 6b shows that the equatorward flow bursts were localized to the eastern portion of the radar FOV. This flow sequence is consistent with the idea that localized fast flows toward the near-Earth plasma sheet field lines lead to substorm onset. While the existence of such preonset flows has been inferred from auroral streamer propagations in previous studies, the radar observations provided direct evidence that fast flows reach the growth phase arc near the onset location just prior to substorm onset.

It is not clear from the current observations whether the first three flow bursts also contributed to the onset. While the density and luminosity show modulations around the times of those flow bursts, it is difficult to distinguish these changes from waves that are discussed below in section 3.3. According to our previous study [*Nishimura et al.*, 2011a], those preceding flow bursts lead to an increase in the luminosity of the growth phase arc, which suggests that they may lead to increases in plasma pressure or pressure gradients in the near-Earth plasma sheet, and this may help to set up the conditions for the last flow burst to lead to onset.

3.3. Waves Along the Growth Phase Arc and Growth to Onset Beads

As shown in Figure 3, the growth phase arc is not a completely quiet, homogeneous arc but has weak intensity modulations that propagate along the arc. Figure 6c shows the altitude distribution of the radar density data within the growth phase arc that lies equatorward of the gray lines in Figure 6a. The peak density at ~200–250 km is not constant but can be seen to oscillate with ~1–3 min periodicity. The lowest altitude of the ionization also goes down in correlation with the peak density enhancements, indicating that both the energy flux and energy of precipitating electrons increase quasi-periodically. The density oscillations do not

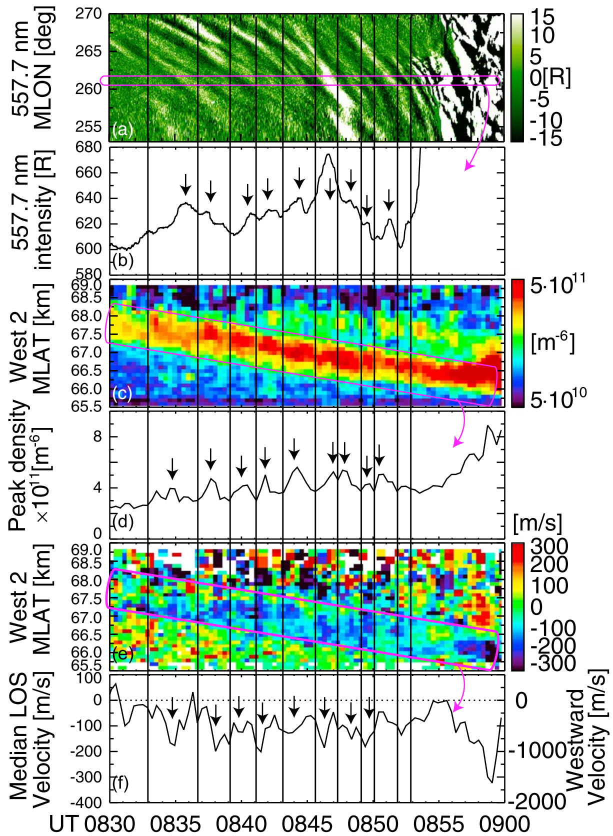

Figure 8. Comparison between preonset waves in optical and radar data. (a) Detrended east-west keogram and (b) line plot of intensity at 261.5° MLON in 557.7 nm data. (c) Latitudinal density distribution and (d) its peak density in the growth phase arc of the West 2 beams. (e) Latitudinal velocity distribution and median velocity in the growth phase arc of the West 2 beams. The right axis shows the westward flow speed assuming that the LOS speed is a projection of a pure westward flow.

occur simultaneously in five meridians but instead propagate westward as highlighted by the black lines. The westward propagation speed of the density based on the slope of the lines is ~1–1.6 km/s.

We investigate these preonset oscillations in more detail using the optical data. Figures 7a, 7b, and 7d show, respectively, north-south keograms along the onset meridian (263° MLON at the onset latitude) from the white-light imager at Fort Yukon and the 630.0 and 557.7 nm data from Poker Flat. Here the imager data were averaged only 0.01° MLON to identify the intensity variations more clearly. The white-light and 557.7 nm data show remarkable intensity oscillations as indicated by the yellow arrows. The oscillation signature in the 630.0 nm wavelength is much weaker, which is expected because of the longer lifetime of emissions at high altitudes [*Omholt*, 1960]. We set sliding windows along the growth phase arc as shown in Figures 7b and 7d and calculated the maximum intensity at each longitude and time. We also subtracted 3 min averages, and the results are shown in Figures 7c and 7e for the 630.0 nm and 557.7 nm data, respectively. The 630.0 nm data show weak (~5 R) but significant westward propagating intensity oscillations with ~2–3 min periodicity. The 557.7 nm data show more structured intensity oscillations that occasionally reached 20 R. The blue and magenta lines visually trace the intensity oscillations, and their slopes indicate that the optical propagation speed is ~1.0–1.3 km/s westward, in reasonable agreement with the radar density propagation speed estimated above. The azimuthal size of each luminosity enhancement is ~100–150 km.

Note that these are not pseudobreakups. The luminosity changes are much smaller than typical auroral initial brightening and did not grow in time. The substorm growth phase is still proceeding as can be seen from the equatorward moving growth phase arc. Rather, these appear to be quasi-stable waves propagating westward and localized along the growth phase arc.

The substorm onset can be seen as an abrupt intensification of three longitudinally separated intensifications. This can be seen more clearly in Figure 7f, which expands the 557.7 nm observations from 0846 to 0856 UT. These intensifications became the beads that signify the initial substorm auroral brightening. Interestingly, these beads can be traced backward in time and are connected to the last three preonset waves, which can be seen to have suddenly intensified at the onset time and turned into the onset beads. This connection suggests that the preonset waves made a transition from stably oscillating to rapidly growing, indicating that the preonset waves are an essential feature of the development of substorm onset instability.

Finally, we compare the optical and radar signatures of the preonset waves in Figure 8. We took the radar data from the West 2 meridian, for which the radar LOS direction is closer to the arc orientation than for the central three radar beam meridians. The peak ionospheric density and median LOS flow velocity within the growth phase arc latitudes are shown in Figures 8d and 8f, respectively. Figure 8b shows the slice of the 5577 nm east-west keogram data at a longitude near the crossing of the growth phase arc and the radar beams (261.5° MLON).

The luminosity, density, and velocity show oscillations with roughly the same timing, supporting the result that the radar and imager detected the same preonset waves. The apparent small phase shifts are likely due to the time-varying density profile in altitude as shown in Figure 6c (the mapping altitude of optical data is fixed to 150 km). If the radar velocity measures the LOS component of purely westward flows, the ~ −200 m/s LOS flow corresponds to a ~1000 m/s westward flow (right vertical axis). Although north-south and vertical flow magnitudes are not considered in this estimation, those components are expected to be weak based on the small flow magnitudes along the central meridian (Figure 6b). Thus, the LOS flow measurements suggest that the preonset density and optical waves are associated westward ionospheric flows roughly with same propagation speed.

4. Conclusion

During the well-instrumented PINOT campaign, a substorm event initiated within the PFISR FOV in excellent coordination with colored and white-light auroral imaging. Since the auroral oval was very thin, the entire latitudinal extent of the auroral oval lay within the radar FOV, allowing the radar to detect the whole event sequence within the auroral oval around the onset meridian. This isolated substorm was preceded by a PBI that was detected as a brightening of the polewardmost auroral arc and enhanced density. Multiple fast flows were found to originate from the polar cap and to propagate across the PBI. The flows were localized azimuthally and reached the growth phase arc within a few degrees in longitude from the substorm auroral onset location just before the substorm onset. This sequence supports the idea that localized earthward flow bursts toward the near-Earth plasma sheet lead to substorm onset and has been suggested from spacecraft [e.g., *Angelopoulos et al*., 2008; *Xing et al*., 2010]. Moreover, our observations directly showed a continuous sequence of preonset flows that propagated from the open field lines into the plasma sheet across the open-closed field line boundary and reached the near-Earth plasma sheet, while in previous studies only a part of the flow sequence was seen or the flow was inferred indirectly from auroral streamer motion [*Nishimura et al*., 2010a, 2010b; *Lyons et al*., 2011].

PFISR also revealed that the growth phase arc is a tall ionization structure that extends between ~150 and ~350 km and that the initial brightening is characterized as enhanced ionization below 200 km. This altitude profile suggests that the growth phase arc is associated with precipitation with a broad energy range and that the initial brightening is due to high-energy precipitation without significant changes in low-energy precipitation.

The density and auroral luminosity along the growth phase arc were not uniform but showed quasi-periodic oscillations with ~1–3 min periods and ~1 km/s westward propagations. Those parameters are consistent with earlier findings by *Uritsky et al*. [2009] and *Panov et al*. [2012]. Those preonset waves remained weak and stable until the onset time and then rapidly intensified as onset beads. Those beads are not a separate auroral form but can be traced backward in time to the faint preonset waves. This connection raises an important implication that the preonset waves are precursors of the substorm onset instability (onset beads formation). Combined with the preonset fast flows mentioned above, our observations suggest that the preonset waves in the near-Earth plasma sheet become unstable as a result of their interaction with the plasma carried by the earthward flow bursts. We thus suggest that the coupling between the earthward flows from farther downtail and the azimuthally propagating waves in the near-Earth plasma sheet leads to the substorm onset instability.

While our ionospheric observations do not allow us to identify the nature of the magnetospheric substorm onset instability, these observations give information about the preonset waves that appear to be driven to instability by the flowing bursts of plasma that intrude into the inner plasma sheet region connecting to the preonset waves. Specifically, the PFISR observations showed enhanced flows, elevated densities, and reduced altitudes of the density associated with the preonset waves. Those indicate that the preonset waves involve formation of quasi-periodic fast azimuthal flows and precipitation with increased flux and energy. Existence of the quasi-periodic flow enhancements in a limited latitude range around the growth phase arc indicates a modulating flow shear in the plasma sheet. It is thus likely that the onset instability is associated with modulations of flows and field-aligned currents, so that an instability such as the shear-flow ballooning instability [*Voronkov et al*., 1997] or kinetic ballooning instability [*Pritchett and Coroniti*, 2010] could be a potential candidate for explaining the observed optical and radar signatures. Further investigations particularly with simultaneous magnetotail observations are needed to determine the onset instability uniquely.

Acknowledgments
This work was supported by NASA grants NNX12AJ57G, NNX09AI06G, and NAS5-02099; NSF grants AGS-1101903, AGS-1042255, AGS-1242356 AGS-1004736, and AGS-1242913; and CSA contract 9F007-046101. PFISR is operated by SRI International on behalf of the NSF under Cooperative Agreement AGS-1133009. THEMIS ASI data are publicly available at http://themis.ssl.berkeley.edu. PFISR and colored ASI data are obtained from M. Nicolls, R. Michell, and M. Samara.

Michael Liemohn thanks the reviewers for their assistance in evaluating this paper.

References

Akasofu, S.-I. (1964), The development of the auroral substorm, *Planet. Space Sci.*, *12*, 273.

Angelopoulos, V., et al. (2008), Tail reconnection triggering substorm onset, *Science*, *321*, 931.

Baker, D. N., et al. (2002), Timing of magnetic reconnection initiation during a global magnetospheric substorm onset, *Geophys. Res. Lett.*, *29*(24), 2190, doi:10.1029/2002GL015539.

Birn, J., J. Raeder, Y. Wang, R. Wolf, and M. Hesse (2004), On the propagation of bubbles in the geomagnetic tail, *Ann. Geophys.*, *22*(5), 1773–1786.

Deehr, C., and D. Lummerzheim (2001), Ground-based optical observations of hydrogen emission in the auroral substorm, *J. Geophys. Res.*, *106*(A1), 33–44, doi:10.1029/2000JA002010.

Donovan, E., et al. (2006), The THEMIS all-sky imaging array—System design and initial results from the prototype imager, *J. Atmos. Sol. Terr. Phys.*, *68*(13), 1472–1487.

Henderson, M. G., G. D. Reeves, and J. S. Murphree (1998), Are north–south aligned auroral structures an ionospheric manifestation of bursty bulk flows?, *Geophys. Res. Lett.*, *25*(19), 3737–3740, doi:10.1029/98GL02692.

Henderson, M. G. (2009), Observational evidence for an inside-out substorm onset scenario, *Ann. Geophys.*, *27*, 2129–2140.

Kauristie, K., V. A. Sergeev, O. Amm, M. V. Kubyshkina, J. Jussila, E. Donovan, and K. Liou (2003), Bursty bulk flow intrusion to the inner plasma sheet as inferred from auroral observations, *J. Geophys. Res.*, *108*(A1), 1040, doi:10.1029/2002JA009371.

Kepko, L., E. Spanswick, V. Angelopoulos, E. Donovan, J. McFadden, K.-H. Glassmeier, J. Raeder, and H. J. Singer (2009), Equatorward moving auroral signatures of a flow burst observed prior to auroral onset, *Geophys. Res. Lett.*, *36*, L24104, doi:10.1029/2009GL041476.

Liang, J., E. F. Donovan, W. W. Liu, B. Jackel, M. Syrjäsuo, S. B. Mende, H. U. Frey, V. Angelopoulos, and M. Connors (2008), Intensification of preexisting auroral arc at substorm expansion phase onset: Wave-like disruption during the first tens of seconds, *Geophys. Res. Lett.*, *35*, L17S19, doi:10.1029/2008GL033666.

Lui, A. T. Y. (1995), Observed features in current disruption and their implications to existing theories, in *Space Plasmas: Coupling Between Small and Medium Scale Processes*, AGU Monograph, vol. 86, 149 pp., AGU, Washington, D. C.

Lyons, L. R., Y. Nishimura, X. Xing, V. Angelopoulos, S. Zou, D. Larson, J. McFadden, A. Runov, S. Mende, and K. H. Fornacon (2010), Enhanced transport across entire length of plasma sheet boundary field lines leading to substorm onset, *J. Geophys. Res.*, *115*, A00I07, doi:10.1029/2010JA015831.

Lyons, L. R., Y. Nishimura, H.-J. Kim, E. Donovan, V. Angelopoulos, G. Sofko, M. Nicolls, C. Heinselman, J. M. Ruohoniemi, and N. Nishitani (2011), Possible connection of polar cap flows to pre- and post-substorm onset PBIs and streamers, *J. Geophys. Res.*, *116*, A12225, doi:10.1029/2011JA016850.

Lyons, L. R., Y. Nishimura, E. Donovan, and V. Angelopoulos (2013), Distinction between auroral substorm onset and traditional ground magnetic onset signatures, *J. Geophys. Res. Space Physics*, *118*, 4080–4092, doi:10.1002/jgra.50384.

Machida, S., Y. Miyashita, A. Ieda, M. Nose, D. Nagata, K. Liou, T. Obara, A. Nishida, Y. Saito, and T. Mukai (2009), Statistical visualization of the Earth's magnetotail based on Geotail data and the implied substorm model, *Ann. Geophys.*, *27*(3), 1035–1046.

Mende, S. B., S. E. Harris, H. U. Frey, V. Angelopoulos, C. T. Russell, E. Donovan, B. Jackel, M. Greffen, and L. M. Peticolas (2008), The THEMIS array of ground-based observatories for the study of auroral substorms, *Space Sci. Rev.*, *141*, 357–387.

Miyashita, Y., et al. (2009), A state-of-the-art picture of substorm-associated evolution of the near-Earth magnetotail obtained from superposed epoch analysis, *J. Geophys. Res.*, *114*, A01211, doi:10.1029/2008JA013225.

Motoba, T., K. Hosokawa, A. Kadokura, and N. Sato (2012), Magnetic conjugacy of northern and southern auroral beads, *Geophys. Res. Lett.*, *39*, L08108, doi:10.1029/2012GL051599.

Nakamura, R., W. Baumjohann, R. Schödel, M. Brittnacher, V. A. Sergeev, M. Kubyshkina, T. Mukai, and K. Liou (2001), Earthward flow bursts, auroral streamers, and small expansions, *J. Geophys. Res.*, *106*, 10,791–10,802, doi:10.1029/2000JA000306.

Nicolls, M. J., and C. J. Heinselman (2007), Three-dimensional measurements of traveling ionospheric disturbances with the Poker Flat incoherent scatter radar, *Geophys. Res. Lett.*, *34*, L21104, doi:10.1029/2007GL031506.

Nishimura, Y., L. Lyons, S. Zou, V. Angelopoulos, and S. Mende (2010a), Substorm triggering by new plasma intrusion: THEMIS all-sky imager observations, *J. Geophys. Res.*, *115*, A07222, doi:10.1029/2009JA015166.

Nishimura, Y., et al. (2010b), Preonset time sequence of auroral substorms: Coordinated observations by all-sky imagers, satellites, and radars, *J. Geophys. Res.*, *115*, A00I08, doi:10.1029/2010JA015832.

Nishimura, Y., L. R. Lyons, V. Angelopoulos, T. Kikuchi, S. Zou, and S. B. Mende (2011a), Relations between multiple auroral streamers, pre-onset thin arc formation, and substorm auroral onset, *J. Geophys. Res.*, *116*, A09214, doi:10.1029/2011JA016768.

Nishimura, Y., L. Lyons, S. Zou, V. Angelopoulos, and S. Mende (2011b), Categorization of the time sequence of events leading to substorm onset based on THEMIS all-sky imager observations, in *The Dynamic Magnetosphere*, IAGA Special Sopron Book Series 3, vol. 113, edited by W. Liu and M. Fujimoto, pp. 133–142, Springer, Netherlands.

Ohtani, S., K. Takahashi, T. Higuchi, A. Lui, H. Spence, and J. Fennell (1998), AMPTE/CCE-SCATHA simultaneous observations of substorm-associated magnetic fluctuations, *J. Geophys. Res.*, *103*(A3), 4671–4682, doi:10.1029/97JA03239.

Omholt, A. (1960), The time delay of the red [OI] lines in the aurora, *Planet. Space Sci.*, *2*, 246–248.

Panov, E. V., V. A. Sergeev, P. L. Pritchett, F. V. Coroniti, R. Nakamura, W. Baumjohann, V. Angelopoulos, H. U. Auster, and J. P. McFadden (2012), Observations of kinetic ballooning/interchange instability signatures in the magnetotail, *Geophys. Res. Lett.*, *39*, L08110, doi:10.1029/2012GL051668.

Pitkänen, T., A. T. Aikio, and L. Juusola (2013), Observations of polar cap flow channel and plasma sheet flow bursts during substorm expansion, *J. Geophys. Res. Space Physics*, *118*, 774–784, doi:10.1002/jgra.50119.

Pritchett, P. L., and F. V. Coroniti (2010), A kinetic ballooning/interchange instability in the magnetotail, *J. Geophys. Res.*, *115*, A06301, doi:10.1029/2009JA014752.

Rae, I. J., C. E. J. Watt, I. R. Mann, K. R. Murphy, J. C. Samson, K. Kabin, and V. Angelopoulos (2010), Optical characterization of the growth and spatial structure of a substorm onset arc, *J. Geophys. Res.*, *115*, A10222, doi:10.1029/2010JA015376.

Rostoker, G., S.-I. Akasofu, J. Foster, R. A. Greenwald, A. T. Y. Lui, Y. Kamide, K. Kawasaki, R. L. McPherron, and C. T. Russell (1980), Magnetospheric substorms—Definition and signatures, *J. Geophys. Res.*, *85*, 1663–1668, doi:10.1029/JA085iA04p01663.

Samara, M., and R. G. Michell (2010), Ground-based observations of diffuse auroral frequencies in the context of whistler mode chorus, *J. Geophys. Res.*, *115*, A00F18, doi:10.1029/2009JA014852.

Samson, J. C., L. R. Lyons, P. T. Newell, F. Creutzberg, and B. Xu (1992), Proton aurora and substorm intensifications, *Geophys. Res. Lett.*, *19*, 2167–2170, doi:10.1029/92GL02184.

Saito, M. H., Y. Miyashita, M. Fujimoto, I. Shinohara, Y. Saito, K. Liou, and T. Mukai (2008), Ballooning mode waves prior to substorm-associated dipolarizations: Geotail observations, *Geophys. Res. Lett.*, *35*, L07103, doi:10.1029/2008GL033269.

Sergeev, V. A., et al. (2000), Multiple-spacecraft observation of a narrow transient plasma jet in the Earth's plasma sheet, *Geophys. Res. Lett.*, *27*, 851–854, doi:10.1029/1999GL010729.

Sergeev, V. A., V. Angelopoulos, D. G. Mitchell, and C. T. Russell (1995), In situ observations of magnetotail reconnection prior to the onset of a small substorm, *J. Geophys. Res.*, *100*(A10), 19,121–19,133, doi:10.1029/95JA01471.

Shi, Y., E. Zesta, L. R. Lyons, J. Yang, A. Boudouridis, Y. S. Ge, J. M. Ruohoniemi, and S. Mende (2012), Two-dimensional ionospheric flow pattern associated with auroral streamers, *J. Geophys. Res.*, *117*, A02208, doi:10.1029/2011JA017110.

Shiokawa, K., et al. (1998), High-speed ion flow, substorm current wedge, and multiple Pi 2 pulsations, *J. Geophys. Res.*, *103*(A3), 4491–4507, doi:10.1029/97JA01680.

Shiokawa, K., I. Shinohara, T. Mukai, H. Hayakawa, and C. Z. Cheng (2005), Magnetic field fluctuations during substorm-associated dipolarizations in the nightside plasma sheet around $X = -10$ RE, *J. Geophys. Res.*, *110*, A05212, doi:10.1029/2004JA010378.

Takahashi, K., L. J. Zanetti, R. E. Lopez, R. W. McEntire, T. A. Potemra, and K. Yumoto (1987), Disruption of the magnetotail current sheet observed by AMPTE/CCE, *Geophys. Res. Lett.*, *14*, 1019–1022, doi:10.1029/GL014i010p01019.

Uritsky, V. M., J. Liang, E. Donovan, E. Spanswick, D. Knudsen, W. Liu, J. Bonnell, and K. H. Glassmeier (2009), Longitudinally propagating arc wave in the pre-onset optical aurora, *Geophys. Res. Lett.*, *36*, L21103, doi:10.1029/2009GL040777.

Voronkov, I., R. Rankin, P. Frycz, V. T. Tikhonchuk, and J. C. Samson (1997), Coupling of shear flow and pressure gradient instabilities, *J. Geophys. Res.*, *102*(A5), 9639–9650, doi:10.1029/97JA00386.

Xing, X., L. Lyons, Y. Nishimura, V. Angelopoulos, D. Larson, C. Carlson, J. Bonnell, and U. Auster (2010), Substorm onset by new plasma intrusion: THEMIS spacecraft observations, *J. Geophys. Res.*, *115*, A10246, doi:10.1029/2010JA015528.

Yang, J., F. R. Toffoletto, R. A. Wolf, S. Sazykin, P. A. Ontiveros, and J. M. Weygand (2012), Large-scale current systems and ground magnetic disturbance during deep substorm injections, *J. Geophys. Res.*, *117*, A04223, doi:10.1029/2011JA017415.

